The Astrophysical Journal, 742:102 (11pp), 2011 December 1 doi:10.1088/0004-637X/742/2/102

OBSERVATIONS OF THE 2006 DECEMBER 13 AND 14 SOLAR PARTICLE EVENTS IN THE 80 MeV n^{-1}–3 GeV n^{-1} RANGE FROM SPACE WITH THE PAMELA DETECTOR

O. Adriani[1,2], G. C. Barbarino[3,4], G. A. Bazilevskaya[5], R. Bellotti[6,7], M. Boezio[8], E. A. Bogomolov[9], L. Bonechi[1,2], M. Bongi[2], V. Bonvicini[8], S. Borisov[10,11,12], S. Bottai[2], A. Bruno[6,7], F. Cafagna[7], D. Campana[4], R. Carbone[4,11], P. Carlson[13], M. Casolino[10,14], G. Castellini[15], L. Consiglio[4], M. P. De Pascale[10,11], C. De Santis[10,11], N. De Simone[10,11], V. Di Felice[10,11], V. Formato[8,16], A. M. Galper[12], L. Grishantseva[12], W. Gillard[13], G. Jerse[8,16], A. V. Karelin[12], S. V. Koldashov[12], S. Y. Krutkov[9], A. N. Kvashnin[5], A. Leonov[12], V. Malakhov[12], L. Marcelli[10], A. G. Mayorov[12], W. Menn[17], V. V. Mikhailov[12], E. Mocchiutti[8], A. Monaco[7], N. Mori[1,2], N. Nikonov[9,10,11], G. Osteria[4], F. Palma[10,11], P. Papini[2], M. Pearce[13], P. Picozza[10,11], C. Pizzolotto[8], M. Ricci[18], S. B. Ricciarini[2], R. Sarkar[8], L. Rossetto[13], M. Simon[17], R. Sparvoli[10,11], P. Spillantini[1,2], Y. I. Stozhkov[5], A. Vacchi[8], E. Vannuccini[2], G. Vasilyev[9], S. A. Voronov[12], J. Wu[13], Y. T. Yurkin[12], G. Zampa[8], N. Zampa[8], and V. G. Zverev[12]

[1] Department of Physics, University of Florence, I-50019 Sesto Fiorentino, Florence, Italy
[2] INFN, Sezione di Florence, I-50019 Sesto Fiorentino, Florence, Italy
[3] Department of Physics, University of Naples "Federico II," I-80126 Naples, Italy
[4] INFN, Sezione di Naples, I-80126 Naples, Italy
[5] Lebedev Physical Institute, RU-119991 Moscow, Russia
[6] Department of Physics, University of Bari, I-70126 Bari, Italy
[7] INFN, Sezione di Bari, I-70126 Bari, Italy
[8] INFN, Sezione di Trieste, I-34149 Trieste, Italy
[9] Ioffe Physical Technical Institute, RU-194021 St. Petersburg, Russia
[10] INFN, Sezione di Rome Tor Vergata, I-00133 Rome, Italy
[11] Department of Physics, University of Rome Tor Vergata, I-00133 Rome, Italy
[12] National Research Nuclear University "MEPhI," RU-115409 Moscow, Russia
[13] KTH, Department of Physics, and the Oskar Klein Centre for Cosmoparticle Physics, AlbaNova University Centre, SE-10691 Stockholm, Sweden
[14] RIKEN, Advanced Science Institute, Wako-shi, Japan
[15] IFAC, I-50019 Sesto Fiorentino, Florence, Italy
[16] Department of Physics, University of Trieste, I-34147 Trieste, Italy
[17] Department of Physics, Universitat Siegen, D-57068 Siegen, Germany
[18] INFN, Laboratori Nazionali di Frascati, I-00044 Frascati, Italy
Received 2011 May 19; accepted 2011 July 19; published 2011 November 14

ABSTRACT

We present the space spectrometer PAMELA observations of proton and helium fluxes during the 2006 December 13 and 14 solar particle events. This is the first direct measurement of the solar energetic particles in space with a single instrument in the energy range from ∼80 MeV n^{-1} up to ∼3 GeV n^{-1}. For the December 13 event, measured energy spectra of solar protons and helium are compared with results obtained by neutron monitors and other detectors. Our measurements show a spectral behavior different from those derived from the neutron monitor network. No satisfactory analytical fitting was found for the energy spectra. During the first hours of the December 13 event, solar energetic particles spectra were close to the exponential form, demonstrating rather significant temporal evolution. Solar He with energy up to 1 GeV n^{-1} was recorded on December 13. For the December 14 event, energy of solar protons reached 600 MeV, whereas the maximum energy of He was below 100 MeV n^{-1}. The spectra were slightly bent in the lower energy range and preserved their form during the second event. Differences in the particle flux appearance and temporal evolution of these two events may argue for special conditions leading to the acceleration of solar particles up to relativistic energies.

Key words: space vehicles: instruments – Sun: coronal mass ejections (CMEs) – Sun: flares

Online-only material: color figures

1. INTRODUCTION

The PAMELA spectrometer (Picozza et al. 2007) is a space instrument designed for the study of primary charged particles and antiparticles in a wide energy interval, mainly from tens of MeV to ≈1.2 TeV for protons. It was launched in an elliptical orbit at an altitude between 350 and 610 km and an inclination of 70° in 2006 June. The main scientific goals of PAMELA are the measurement of the particle and antiparticle component in Galactic cosmic rays (Adriani et al. 2009a, 2009b) and the study of Galactic cosmic ray modulation by solar activity and solar energetic particles (SEPs; Casolino et al. 2006a; De Simone et al. 2009). This paper reports the PAMELA measurements of the solar proton and helium fluxes in the energy range from below 100 MeV n^{-1} to several GeV n^{-1} during the 2006 December 13 and 14 solar particle events.

The problem concerning the mechanism and site of SEP acceleration remains an open question. Certainly, SEP may be produced after powerful explosive events on the Sun, accompanied by solar flares, coronal mass ejections (CMEs), bursts of solar X/gamma-rays, and radio emission (Reames 1999). It is clear that a single mechanism is not involved in SEP generation. Stochastic acceleration, shock acceleration, and acceleration by the DC electric fields in the process of magnetic reconnection are the main candidates. The acceleration of SEPs may take place in the flare region, solar corona, and even in

the interplanetary space. It should be kept in mind that SEPs themselves, while propagating, create conditions for energy redistribution (Tylka 2001; Lee 2005). Therefore, the energy spectrum of SEPs provides valuable information for the study of solar and interplanetary plasma processes. Most energetic particles are usually (not always) accelerated during a short time close to the energy explosion, thus the first particles arriving at the observer site retain more information about the primary acceleration process. Less energetic SEPs may be accelerated during hours and even days. Conditions for particle acceleration in the corona and interplanetary space are determined by the temporal and spatial evolution of a shock (e.g., Ellison & Ramaty 1985).

Since the energy range of SEPs extends over more than five orders of magnitude, and SEP fluxes occupy more than eight orders of magnitude, the SEP energy spectrum has never been measured by a single instrument. The bulk of the SEP observations have been performed on spacecraft and cover the particle energy below several hundred MeV n^{-1}, whereas the relativistic solar particles have been observed by ground-based installations and remain less elucidated. This kind of observation and associated modeling can also be used to issue radiation alerts to be used by manned and unmanned missions. A multi-detector study of the solar particle event occurring in 2005 and the corresponding GLE69 was performed on the ground using neutron monitor (NM) and standard radiation environment monitor radiation environment units in space (Papaioannou et al. 2011).

It is not yet clear if relativistic solar particles require a special scenario for their generation. Some authors believe that relativistic solar protons have two components—the fast and the delayed. The fast component is initially accelerated in the flare region (e.g., Vashenyuk et al. 2006, 2008a, 2008b; McCracken & Moraal 2008), probably via magnetic field reconnection, whereas another mechanism, probably shock or stochastic acceleration, generates the second particle component. Bieber et al. (2004, 2005) argue against two components and in favor of the CME-driven shock as a main accelerator of the whole SEP population. A wide variety of concomitant acceleration conditions supports the point that various mechanisms play the main role in different SEP events (Bombardieri et al. 2008; Bazilevskaya 2009). Detailed studies of more solar particle spectra in a wide energy range are needed to resolve this problem.

Since ground-based instruments can only detect secondary cosmic rays, knowledge of the response to the primary particles is necessary in order to find SEP fluxes in space. Some methods were developed (Shea & Smart 1982; Cramp et al. 1997; Bieber et al. 2004; Plainaki et al. 2007; Vashenyuk et al. 2006) to derive energy spectra and angular anisotropy of solar particles using the enhancements in the count rates of NMs. Nevertheless, the particle fluxes derived from the NM data are model dependent.

Before the PAMELA launch, direct measurements of the relativistic solar particles were not fulfilled. The aim of this paper is to present the results of the first direct measurements by a single instrument of the solar protons in the energy range from 80 MeV to several GeV and the helium nuclei from 75 MeV n^{-1} up to ~700 MeV n^{-1} during the SEP events of 2006 December 13 and 14. The absolute intensities and energy spectra are compared with the results of direct (*GOES*, *ACE*) and indirect (NMs, IceTop) measurements.

2. INSTRUMENT DESCRIPTION

The PAMELA spectrometer (Figure 1) consists of a number of highly redundant detectors capable of particle detection through the determination of their charge, mass, rigidity, and velocity over a very wide energy range. The total weight of PAMELA is 470 kg; its power consumption is 355 W.

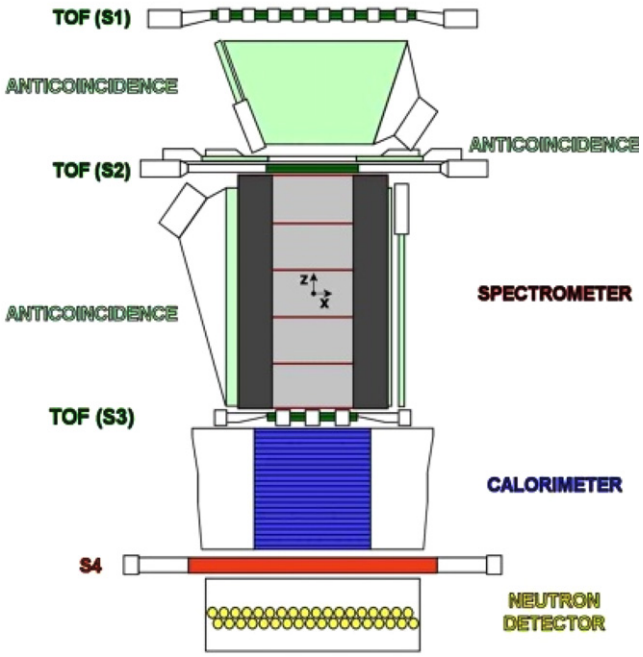

Figure 1. Scheme of the PAMELA instrument. S1, S2, S3—TOF scintillator planes (each plane consists of two layers); anticoincidence system; spectrometer—tracker surrounded with a permanent magnet; silicon–tungsten calorimeter; S4—shower tail catcher, neutron detector. Particles enter the detector from the top, cross the scintillators, and are bent in the magnetic spectrometer before interacting with the calorimeter.

(A color version of this figure is available in the online journal.)

A more detailed description of the device and the data handling can be found in Picozza et al. (2007) and Casolino et al. (2006b, 2006c). The core of the instrument is a spectrometer, constituted of a permanent magnet with a silicon microstrip tracker providing momentum and charge (with sign) information (Adriani et al. 2003). The permanent magnet is 43.66 cm high and is constructed of five modules with high residual magnetic induction (0.43 T), providing an almost constant magnetic field value in the cavity. The tracking system (Ricciarini 2007) is composed of six planes of high-precision Si microstrip detectors, positioned between the five magnetic modules of the tower, with uniform vertical spacing of 8.9 cm. Each silicon plane performs measurements of energy release and track position with a precision of about 3.0 μm (X—bending view) and 11.5 μm (Y view).

A scintillator system (Barbarino et al. 2003) provides trigger, charge, and time of flight (TOF) information. It is composed of three double layers—S1, S2, and S3—divided into various bars for a total of 48 scintillator paddles. It is also used to reject albedo particles that cross the detector from bottom to top.

An anticoincidence system is used to reject spurious events in the offline phase.

A silicon–tungsten calorimeter (Boezio et al. 2002) is used to perform hadron/lepton separation. It is composed of 44 silicon layers interleaved by tungsten planes for a total of 16.3 X_0 (radiation lengths) and 0.6 λ_i (nuclear interaction lengths).

A shower tail catcher (S4) and a neutron detector at the bottom of the apparatus are used to increase lepton/hadron separation.

Around the detectors are housed the readout electronics, the interfaces with the CPU, and all primary and secondary power

supplies. All systems are redundant with the exception of the CPU, which is more tolerant to failures. The system is enclosed in a pressurized container located on one side of the *Resurs-DK1* satellite.

3. DATA SELECTION AND ANALYSIS CRITERIA

3.1. Geometrical Factor and Top of the Payload Correction

The geometrical factor (G_f) of the detector has been evaluated defining a fiducial area consisting of a frame of 0.15 cm from the walls of the $13.1 \times 16.1\,\mathrm{cm}^2$ wide magnetic cavity. Only particles inside this fiducial area have been selected. This reduced volume ensures that all particles entering the magnetic cavity cross the scintillators and do not hit the magnet walls. The value of $G_f = 19.93\,\mathrm{cm}^2\,\mathrm{sr}$, constant within 1%, has been estimated with a numerical calculation and cross-checked with a Monte Carlo simulation in which all the physical interaction processes are inactive, with the exclusion of particle bending in the magnetic field. The two values of G_f have been found to be in agreement within 0.1%.

Interaction losses due to local interactions were taken into account as a scale factor and have been added to the geometrical factor. Protons and helium nuclei may be lost due to scattering and/or hadronic interactions in the 2 mm Al thick pressurized container in which PAMELA is housed, or in the top of the detector. Correction factors amount to $\simeq$6% for protons and $\simeq$12% for He due to the different cross section of the two species.

3.2. Trigger System

In low radiation regions, close to the geomagnetic equator and outside the South Atlantic Anomaly, where PAMELA crosses the trapped protons of the inner Van Allen belt, particles must cross at least one of the two layers of the three scintillator systems (S1, S2, S3) to provide a valid trigger. In low cutoff regions or in the Van Allen belts, where the particle rate is higher, an S1 signal is not required to avoid random triggers due to the high number of particles. Given the low energy of solar particles compared to the galactic nuclei, in this analysis we have used particles selected in high latitude regions and thus taken with only (S2 and S3) configuration.

3.3. Live Time

The live time t_{live} of the apparatus is evaluated using the scintillator and trigger system. The counters for the live and dead time ($t_{\mathrm{live}}, t_{\mathrm{dead}}$) are cross-checked with the onboard time of the CPU, measuring the acquisition time ($t_{\mathrm{acq}} = t_{\mathrm{live}} + t_{\mathrm{dead}}$), to remove possible systematic errors due the counting method. The error associated with clock resolution is negligible compared to other sources of systematic errors.

3.4. Event Selection

3.4.1. Time of Flight System Selection

In this analysis, we have selected events that do not produce secondary particles in the S1 and S2 scintillators and in the tracker, requiring a single fitted track within the spectrometer fiducial acceptance and a maximum of one paddle hit in S1 and S2, matching the extrapolated from the tracker trajectory.

Particles interacting in the satellite can produce showers with different secondaries hitting the scintillator pads. These showers may produce random coincidences in the scintillators: they are rejected by means of anticoincidence and TOF cuts. We require the absence of hits in the anticoincidences around the empty area between S1 and S2 and around the top magnetic cavity (CARD and CAT, respectively). We have placed no constraints on the anticoincidences around the magnet (CAS) and S3, since they are more often hit by backscattered secondaries produced in the calorimeter. The probability of such particles hitting CARD and CAT has been estimated with experimental data and cross-checked with Monte Carlo simulations. This efficiency has been included in the proton flux estimation. No constraints on the anticoincidence have been imposed for helium.

The timing information of the TOF scintillator paddles along the extrapolated trajectory is used to evaluate the β of the particle. Albedo particles crossing the detector from bottom to top are discarded by requiring a positive β.

3.4.2. Proton and Helium Identification

Since average energy loss of a charged particle through matter follows the Bethe Bloch formula, $dE/dx \propto Z^2/\beta^2$ (neglecting logarithmic terms), the measurement of the average energy released in the tracker planes for a given event at a given rigidity can be used to identify different particles. We have selected proton and helium candidates requiring energy loss in the tracker planes compatible with $Z = 1$ and $Z = 2$ nuclei.

Cuts in the energy loss (dE/dx) versus rigidity remove positrons, pions, and particles with $Z \geqslant 2$ as shown in Figure 2. The bands in the figure due to protons and helium nuclei that have energy loss in the tracker $Z^2 = 4$ times protons are identified. Events with small energy losses below 1 GV are due to positrons, also relativistic at low rigidities and the background of secondary pions. The contribution from these two particles is negligible with respect to protons above 1 GV. The black lines show the rigidity-dependent cuts used to select the proton and helium samples. From the same figure the deuterium contribution at low rigidities can also be identified, resulting in a band with energy releases higher than protons. In this work we did not discriminate between isotopes.

Using the redundancy of energy loss measurements in tracker and TOF, residual contamination of protons in the helium sample has been found to be below 0.5% in the energy range used for this work.

3.4.3. Geomagnetic Selection

The high inclination (70°) orbit of the *Resurs-DK1* satellite allows particles of different origin and nature to be studied. To separate the primary (solar and Galactic) component from the reentrant albedo component (particles produced in cosmic ray interactions with the atmosphere below the cutoff and propagating along Earth's magnetic field line), we evaluated the local geomagnetic cutoff G in the Störmer approximation (Shea et al. 1987). The value of $G = 14.9/L^2$—valid for vertically incident particles—was estimated calculating the McIlwain L shell with the International Geomagnetic Reference Field magnetic field model along the orbit (NOAA 2011b). Particles requiring $R > 1.3\,G$ were selected to remove any effect due to directionality in the detector and Earth's penumbral regions.

3.4.4. Tracker Selection

Particle rigidity was obtained fitting its track in the spectrometer. In this analysis, we selected events with a single track fully contained inside the fiducial acceptance.

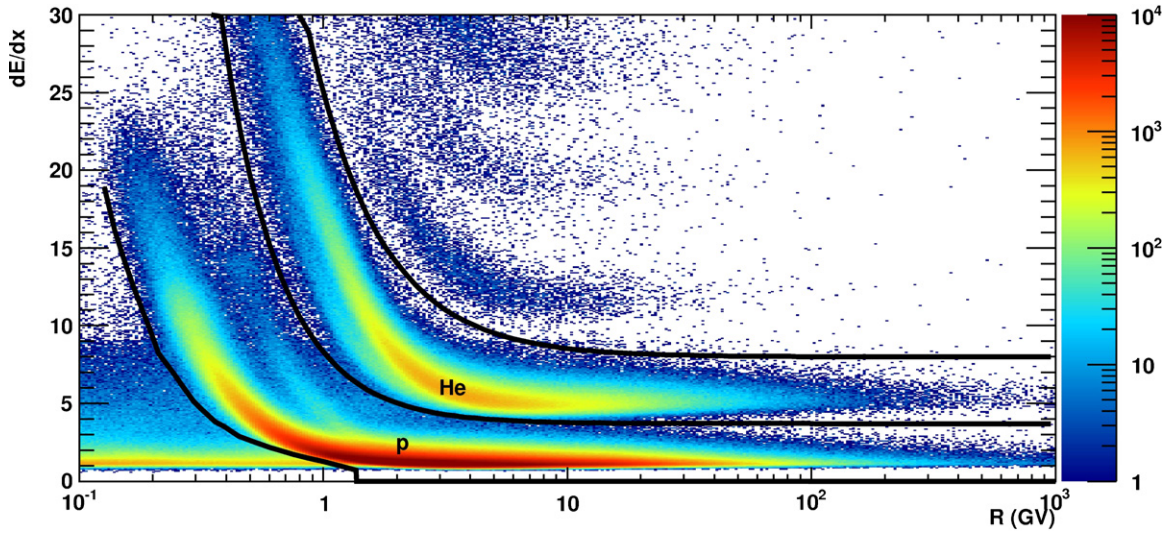

Figure 2. Energy loss (dE/dx) vs. rigidity in the PAMELA tracker. The black lines show the rigidity-dependent cuts used to select proton and helium samples.
(A color version of this figure is available in the online journal.)

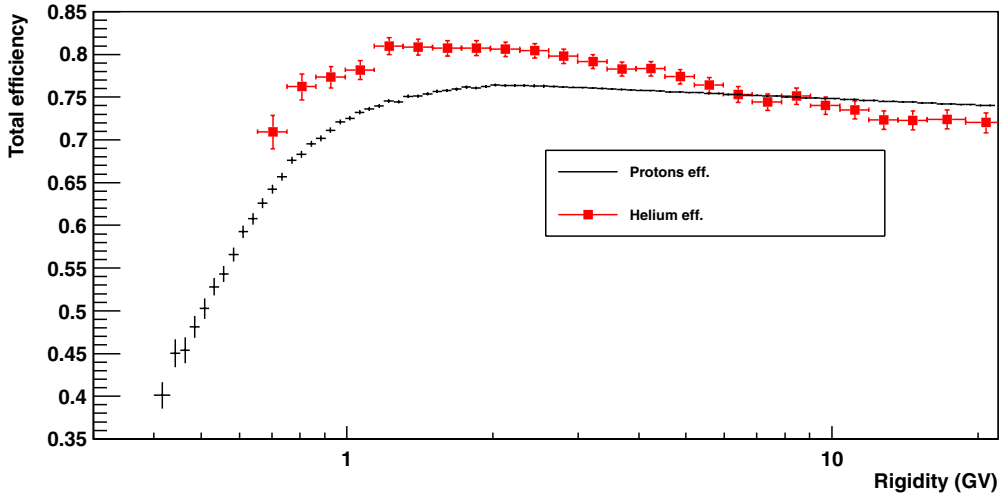

Figure 3. Selection efficiencies for proton and helium particles after all cuts are applied.
(A color version of this figure is available in the online journal.)

For each particle, the tracking system provides up to 12 position measurements (6 in the bending view), which are interpolated with a trajectory evaluated by integrating the equations of motion in the magnetic field. At low rigidities (below $\simeq$1 GV), we have corrected for the energy loss in the detector.

The Maximum Detectable Rigidity (MDR) for a given detector is defined as the rigidity for which the relative error on the rigidity $\Delta R/R = 100\%$ and varies between 200 GV and 1.5 TV, depending on delta-ray production and the event's topology. In this analysis, therefore, the particle rigidity is well below the MDR; thus, no MDR requirements have been applied.

3.4.5. Selection Efficiencies and Residual Contamination

The tracker efficiency has been measured selecting a sample of events that leave straight tracks in the calorimeter and do not interact hadronically. These tracks were propagated back through PAMELA acceptance, and tracker efficiency has been evaluated.

The total selection efficiencies for both species have been obtained as products of tracker, TOF (anticoincidence) efficiencies. The resulting efficiencies for proton and helium nuclei after all above mentioned cuts are shown in Figure 3. For a detailed discussion see Adriani et al. (2011).

Although we put strong requirements on tracker, TOF, and anticoincidence systems, there is nevertheless residual contamination of secondary particles produced on the top of the payload entering the PAMELA acceptance window and passing selection cuts. The maximum contribution to the background for protons comes from secondary single-charge particles (positrons and pions). In the case of helium, the rejection power of our selection cuts is enough to make residual contamination negligible. In order to estimate this contamination, we carried out a 2π Monte Carlo simulation of the protons and helium nuclei hitting the PAMELA pressurized container. Two different hadronic interaction packages, based on Fluka (Battistoni et al. 2007; Ferrari et al. 2005) and Geant 4 (Allison et al. 2006; Agostinelli et al. 2003), have been employed to simulate these interactions. This background decreases with increasing energy and amounts for less than a few percent at 1 GV. Flux attenuation was estimated with an energy-dependent simulation; it is constant above several GV.

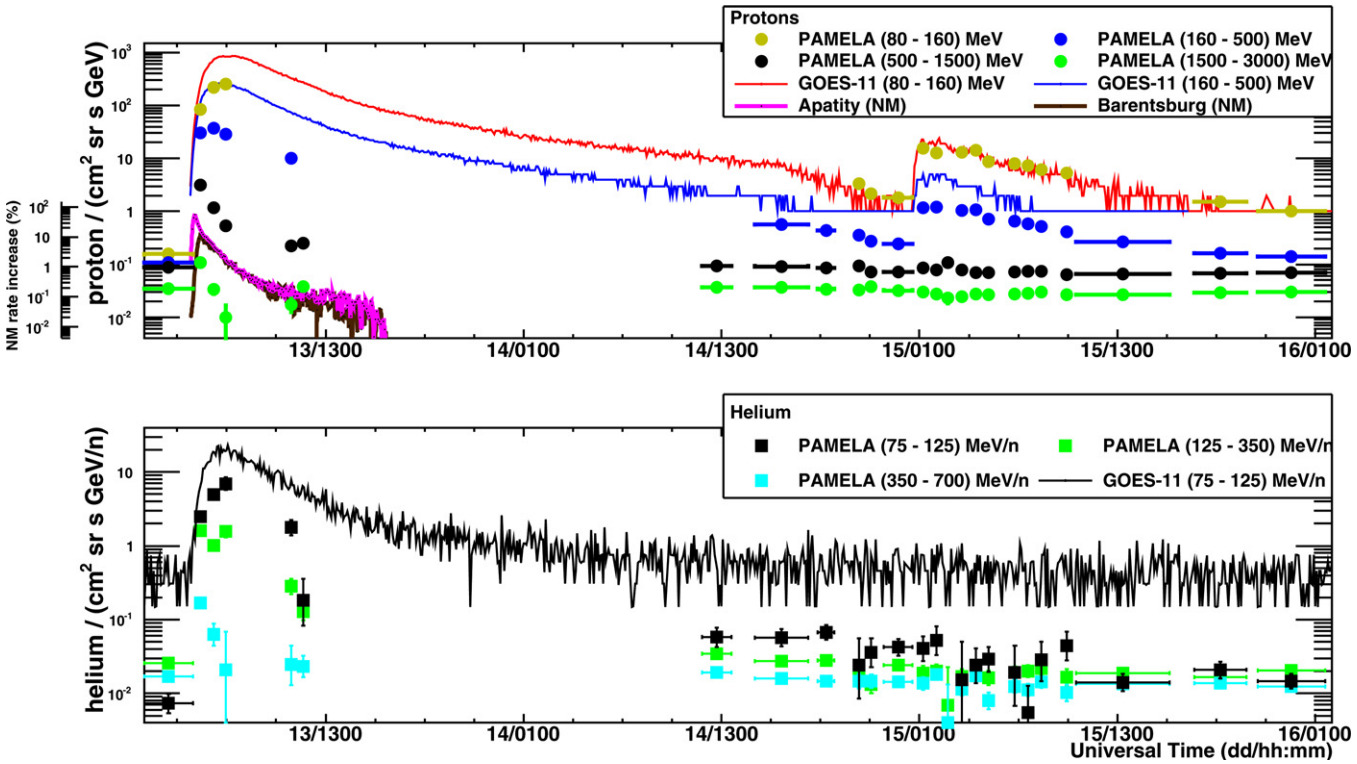

Figure 4. Intensity of solar protons (top panel) and helium (bottom panel) of various energies as a function of time. Top panel: circles are the PAMELA protons in the ranges of 80–160 MeV (yellow), 160–500 MeV (blue), 500–1500 MeV (black), and 1.5–3.0 GeV. (green). Lines are the *GOES 11* protons for 80–160 MeV(red) and 160–500 MeV (blue) ranges. The enhancement in the NM count rates in percents with respect to the background before the event is given for Apatity ($Rc = 0.65$ GV, violet line) and for Barentsburg ($Rc = 0.1$ GV, brown line). Bottom panel: squares are the PAMELA helium in the ranges of 75–125 MeV n^{-1} (black), 125–350 MeV n^{-1} (green), and 350–700 MeV n^{-1} (cyan). The black line is 75–125 MeV n^{-1} He from *GOES 11*.

(A color version of this figure is available in the online journal.)

4. 2006 DECEMBER 13 AND 14 SOLAR PARTICLE EVENTS

4.1. General Description

The most significant SEP fluxes detected by PAMELA started on 2006 December 6, 13, and 14 and originated from the active region NOAA 10930. The December 6 event originated at the East limb, resulting in a gradual proton event reaching the Earth on December 7 and lasting until the events of December 13 and 14. Due to a scheduled maintenance procedure, no data were collected by the PAMELA tracker during the December 6 event, requiring a different analysis approach that will be discussed in a forthcoming paper. On 2006 December 13 at 0214 UT, an X3.4/4B solar flare occurred in the same active region NOAA 10930 (S06W23; NOAA-STP 2006). The intensity of the event was quite unusual for a solar minimum condition. This event also produced a full-halo CME with the sky plane projected speed of 1774 km s^{-1} (Laboratory 2011). The forward shock of the CME reached Earth at 1438 UT on December 14, causing a Forbush decrease of Galactic cosmic ray intensities that lasted for several days.

The flare X1.5 (S06W46) at 2107 UT on December 14 gave start to a new growth of particle intensity as recorded by PAMELA and other satellites. The maximum energy of protons was below 1 GeV, and therefore no ground level enhancement (GLE) was recorded. The corresponding CME had a velocity of 1042 km s^{-1}.

Figure 4 shows the solar particle intensity-time profiles with various energies as observed by the PAMELA spectrometer, *GOES 11*, and NMs. Ground-based NMs started recording SEPs at 0248 UT, while the near-Earth satellites responded later to SEPs of lower energies. The first solar protons arrived at Earth's orbit with anisotropic pitch-angular distribution, which resulted in different intensity-time profiles at NMs situated at locations with the same geomagnetic cutoff R_c but different asymptotic directions of incoming particles. A highly collimated bunch of relativistic solar particles was observed by the muon hodoscope URAGAN at 0256–0304 UT (Timashkov et al. 2008). Anisotropy vanished by 0430 UT (Vashenyuk et al. 2008a).

The whole energy range of SEPs detectable by the PAMELA spectrometer can only be taken in the high latitude regions, where the geomagnetic cutoff is lower than the rigidity of solar particles. Measurements were performed during five passages of PAMELA through the polar regions on December 13. Data were missed from 1000 UT on December 13 until 0914 UT on December 14 because of an onboard system reset of the satellite.

The results of the PAMELA measurement during the 2006 December 13 and 14 SEP events are shown in Figures 5 and 6, respectively. The quiet time Galactic spectra were measured in 2006 November. The first (southern) polar passage of PAMELA started at 0318 UT and showed strong flattening of p and He spectra at energies ~200 MeV n^{-1}. The helium spectrum in the initial phase of the December 13 event is almost similar in shape to the proton one, but flatter at energies below 200 MeV n^{-1}. In the event of December 13 the initial spectra were rather hard and changed significantly at least until 1000 UT. Further evolution of the proton and helium spectra was rather smooth even in spite of a Forbush effect in the middle of December 14, until arrival at ~2300 UT of the SEPs accelerated in the flare at 2107 UT on

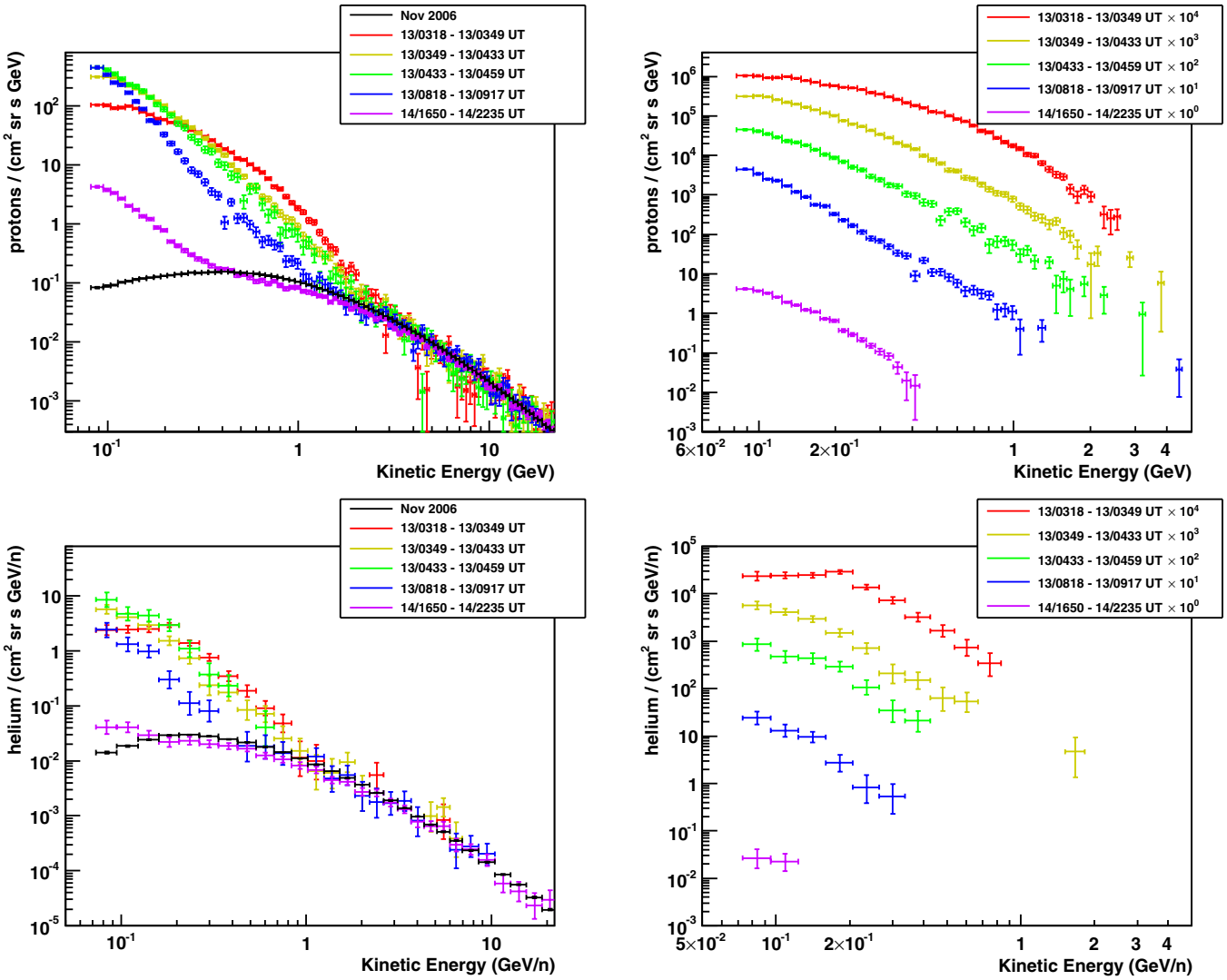

Figure 5. Proton (top panels) and helium (bottom panels) spectra as measured by PAMELA for the SEP event of 2006 December 13. Left: absolute fluxes. Right: after subtraction of Galactic background. Fluxes are scaled to improve separation of curves. In the time slices of December 14, 1650–2235 UT, it is possible to see the Forbush decrease of Galactic particles after the arrival of the CME.

(A color version of this figure is available in the online journal.)

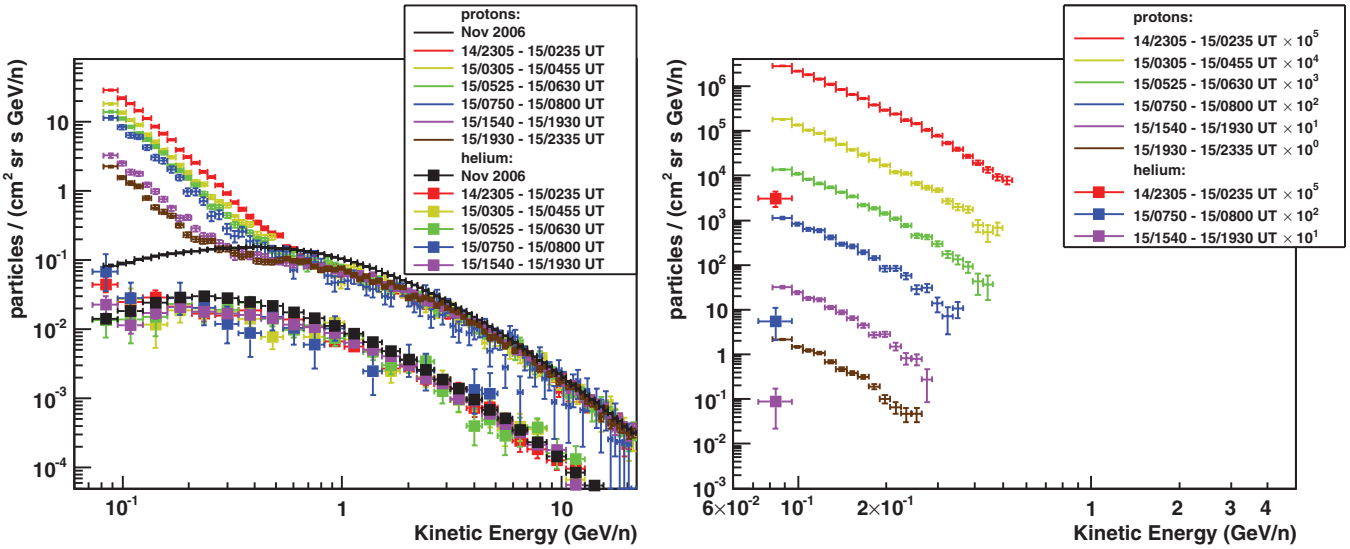

Figure 6. Proton and helium spectra as measured by PAMELA for the SEP event on 2006 December 14. Left: absolute fluxes. Right: after subtraction of Galactic background. Fluxes are scaled to improve separation of curves.

(A color version of this figure is available in the online journal.)

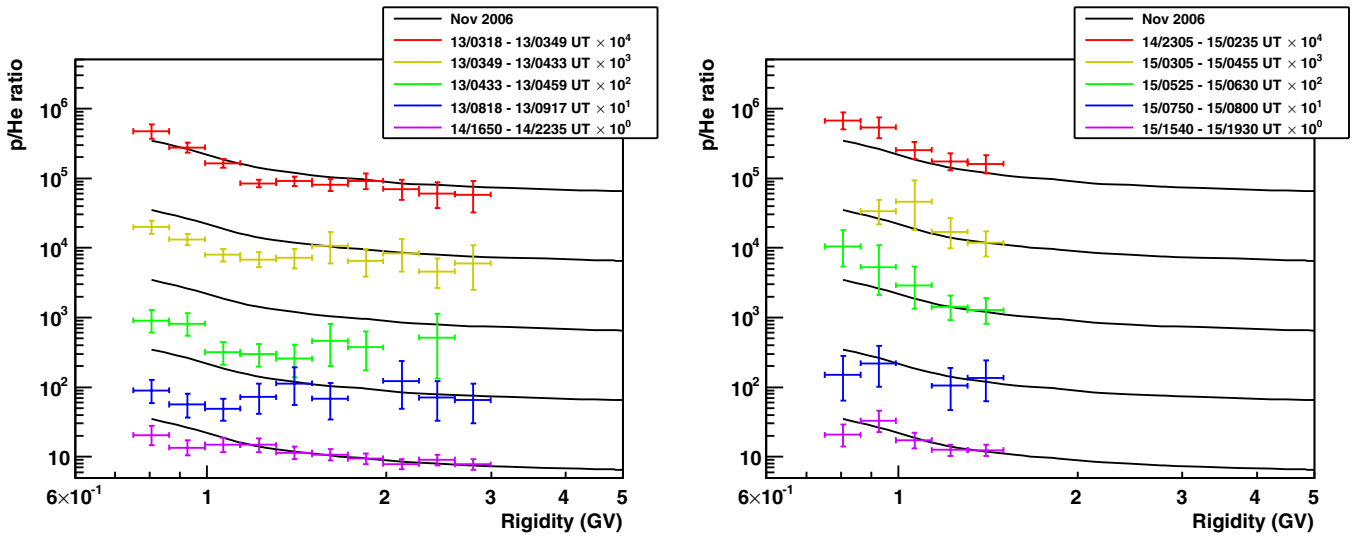

Figure 7. Proton-to-helium ratio vs. rigidity at selected time intervals during the solar events of December 13 (left panel) and December 14 (right panel). The ratios are scaled to clarify the results. The Galactic cosmic ray background is not subtracted, and the ratio observed before the solar events is given as a black line.
(A color version of this figure is available in the online journal.)

December 14. The intensity of ∼100 MeV protons first increased until ∼0400 UT on December 13 and stayed at almost the same level for at least 4 hr, while higher energy particles were rather rapidly removed from Earth's vicinity. After that, the particle intensity decreased, but the spectrum shape was almost constant. Flux intensity did not decrease to the solar quiet levels because of the onset of the December 14 event. During this event the spectral form slightly flattened in the lower energy part, thus remaining quasi-exponential. The highest proton energy for this event was around 500 MeV.

We have examined the temporal behavior of the proton-to-helium ratio in both solar events. For this analysis the rigidity spectra were evaluated with rigidity intervals chosen in accordance with Adriani et al. (2011). Figure 7 presents the proton-to-helium ratio obtained in selected time intervals. The Galactic background was not subtracted and is shown as black curves. It is seen in the left panel of Figure 7 that at the beginning of the December 13 event the ratio was almost the same as for Galactic cosmic rays (note that SEP intensity was highest at that time). The subsequent measurements showed the enhancement of He relative to protons up to late December 14 when the high rigidity He virtually disappeared after subtraction of the Galactic flux. Such behavior may with a first approximation be interpreted as a result of faster removal of solar protons from Earth's orbit. Protons have higher velocity than He of the same rigidity; therefore, the diffusion coefficient of He at the same rigidity is smaller and protons leave more quickly. Further analysis using particle propagation modeling is needed. The right panel of Figure 7 clearly shows that no solar helium with rigidity above 1 GV was observed in the December 14 event.

No analysis directed to search for ^{2}H and ^{3}He has yet been performed. No electrons or positrons of solar origin were found by PAMELA. However, it should be noted that the energy threshold of PAMELA is at ∼50 MeV, which is rather high for solar electrons.

4.2. Initial Phase of the 2006 December 13 Event

The first arriving particles are objects of special interest because they provide more information about the mechanism and conditions of acceleration. As was mentioned, solar particles at the initial phase of the December 13 event demonstrated highly anisotropic angular distribution. In such conditions, the asymptotic directions of particles arriving at PAMELA should be taken into account.

The geomagnetic field acts not only as a rigidity analyzer but also as an angular analyzer of charged particles coming from space. Because of a decline in the geomagnetic field, a particle with certain rigidity above the geomagnetic cutoff R_c can arrive at a given site only from a definite direction outside the magnetosphere (an asymptotic direction). Therefore, at any point of its orbit, PAMELA accepted particles with certain rigidity from only one asymptotic direction.

At the moment of the first particle's arrival, PAMELA was at the latitude of 40° N moving to the equator. Therefore, the low-energy particles could not reach the PAMELA detector. In addition, viewing directions of PAMELA were changed rapidly as the spacecraft moved along the orbit. This can be seen in the upper panel of Figure 8, where the asymptotic directions of 7 GV and 10 GV protons arriving at PAMELA are shown for the initial phase of the SEP event. The asymptotic viewing directions of PAMELA have been calculated with the program developed by B. Gvozdevsky (2009, private communication) using the back-tracing of solar particle trajectories and the magnetospheric model of Tsyganenko (2002). It is in reasonable agreement with what Plainaki et al. (2009b) obtained with the Tsyganenko (1989) model. The direction of the SEP anisotropy axis, i.e., the direction from which the bulk of SEPs comes, is also plotted (Vashenyuk et al. 2008a). According to Figure 8, PAMELA viewing directions at the early phase of the SEP event would allow the solar protons in the range of 7–10 GV to be recorded by PAMELA at 0248–0250 UT, as these particles arrived within a ∼30°cone around the SEP flux axis. However, above 3 GeV the statistic is poor, and we have found no increase of proton flux there. Changes in the viewing directions of PAMELA resulted in a rapid receding of its favorable direction of acceptance from the solar proton anisotropy axis. By 0256 UT (when a collimated particle bunch was observed by Timashkov et al. 2008) the geomagnetic cutoff of PAMELA was 12 GV, and only protons with rigidity between 15 and 17 GV could come from directions close to the anisotropy axis.

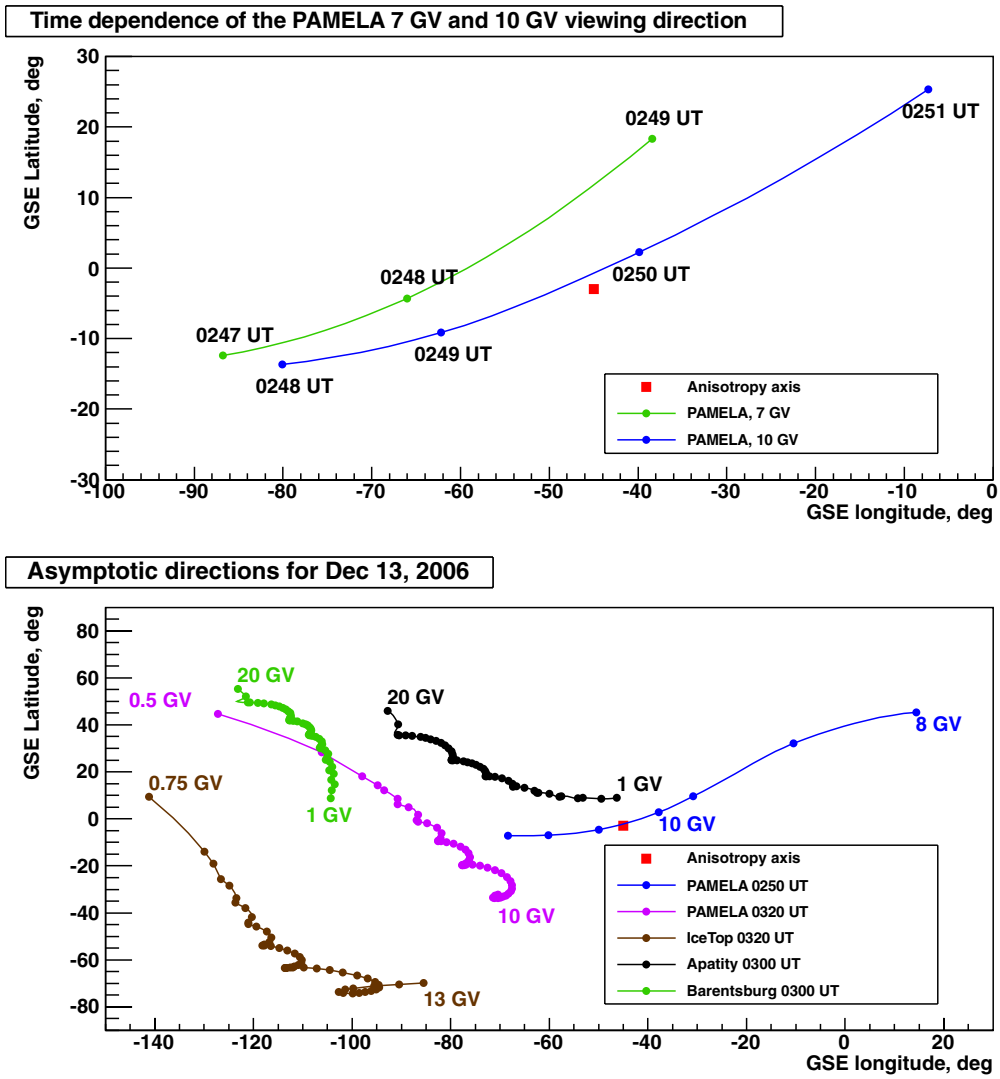

Figure 8. Upper panel: the asymptotic directions of 7 GV and 10 GV protons arriving at PAMELA in the initial phase of the SEP event at selected times of 2006 December 13 (given near the curves). Lower panel: asymptotic directions of protons arriving at PAMELA, the Apatity and Barentsburg NMs, the IceTop installation. The particle rigidity is marked near the corresponding direction. Red squares denote the direction of the SEP anisotropy axis.

(A color version of this figure is available in the online journal.)

The lower panel of Figure 8 shows the asymptotic directions of particles with different energies arriving at PAMELA in the beginning of the event and at the most optimal time of observation when the energy spectrum of particles with energies above ~80 MeV n^{-1} was measured. For comparison, the asymptotic directions for the Apatity NM and for the IceTop installation (Abbasi et al. 2008) are shown in Figure 8.

4.3. Comparison with Other Data

In Figure 9, the differential spectra of PAMELA with the Galactic background subtracted are compared with other experiments. Each panel corresponds to a different time period.

In the low-energy range PAMELA particle fluxes can be compared with other spacecraft measurements. The *GOES* (NOAA 2011a) fluxes are in moderate agreement with the PAMELA ones, with the exception of the most energetic *GOES* band (160–500 MeV), where *GOES* fluxes are several times higher. The same is true for the *GOES* helium spectra. This could be due to contamination of lower energy particles in these *GOES* channels. On the other hand, the PAMELA helium fluxes are in good agreement with measurements performed by the *ACE*/Solar Isotope Spectrometer (SIS; ACE 2011) in the adjacent energy interval.

At high energy, our data can be compared with the IceTop shower array (Abbasi et al. 2008) and the NM network (Vashenyuk et al. 2008a). The results of the IceTop shower array are plotted in Figures 9(a) and (b), specially taken at the time intervals of PAMELA observations (T. Kuwabara 2009, private communication). The IceTop installation has detected secondary particles generated by the SEPs, i.e., the calculated yield functions have been used to reconstruct the primary SEP fluxes. The IceTop results are depicted only in the energy range over which this detector was actually seeing a significant number of particles. The SEP fluxes obtained by PAMELA and those obtained by IceTop are in relatively good agreement. However, at 0318–0329 UT (Figure 9[a]) the power-law shape of the IceTop spectrum does not match the PAMELA spectrum, which is more exponential in nature. At 0406–0420 UT (Figure 9[b]) the spectra of PAMELA and that of IceTop are virtually coincident in the overlapping energy range.

The energy spectra from the NM network have been derived from the early phase of the event (before 0300 UT on

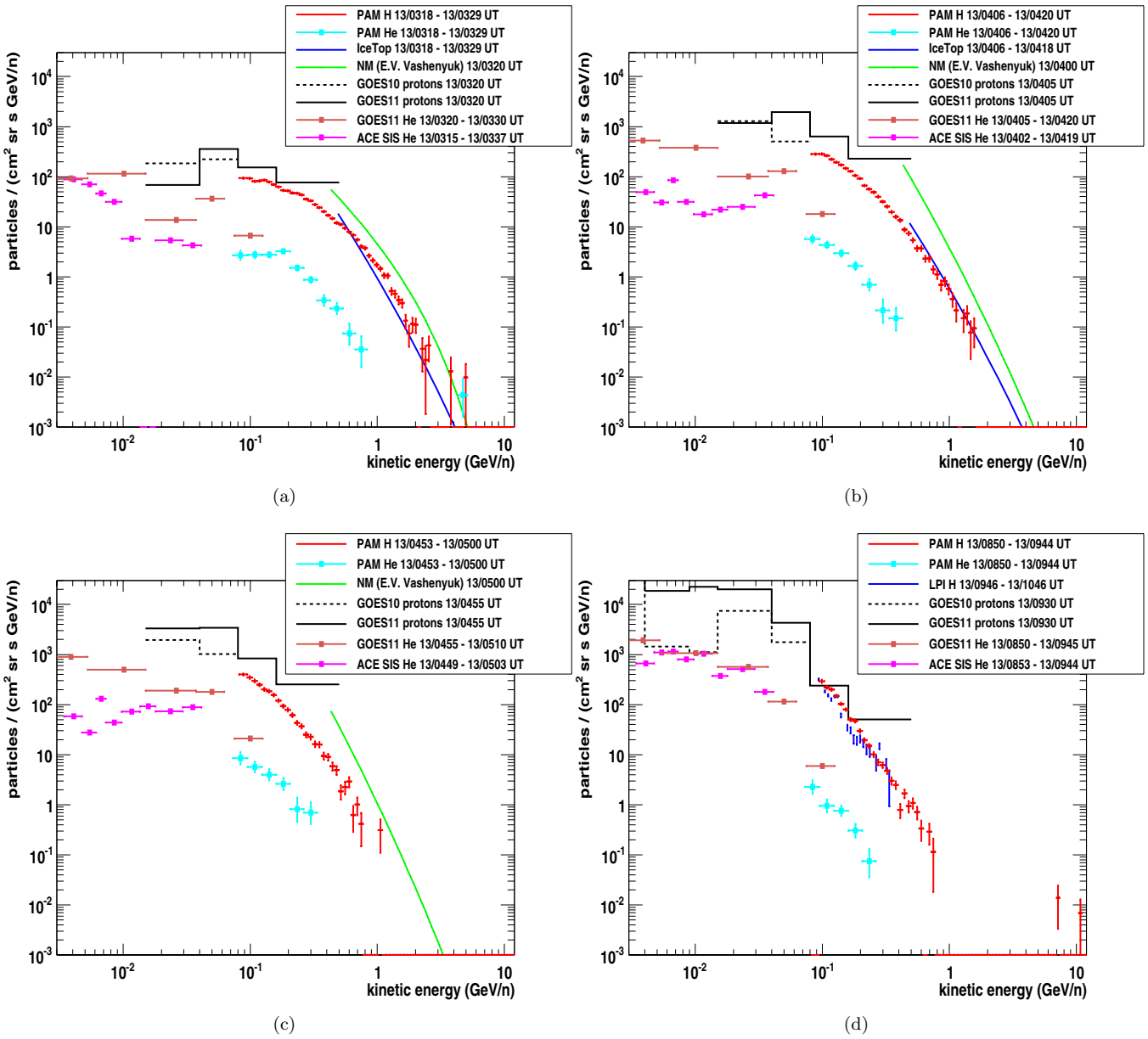

Figure 9. Energy spectra of solar particles measured by the PAMELA spectrometer (with Galactic background subtracted) and by other experiments. In red are the PAMELA protons, in cyan the PAMELA He, and the horizontal bars are the *GOES* and *ACE*/SIS data. (a)–(c): the green line is the spectrum derived from the NM network, and the blue line is the IceTop spectrum; (d): in blue are the LPI balloon data.

(A color version of this figure is available in the online journal.)

December 13) until ∼0500 UT on December 13 (Y. Balabin 2009, private communication). As already mentioned, PAMELA missed the early phase of the event and took the first measurement at 0318–0329 UT, during mildly anisotropic particle arrival (Figure 9[a]). A shape of the PAMELA proton spectrum is close to that derived from the NM network at energies between 700 MeV and 2 GeV. At lower energies the PAMELA spectrum is harder; at $E > 2$ GeV the uncertainty in the PAMELA spectrum is high because of small statistics. The absolute intensities of protons from PAMELA are somewhat lower than those derived from NMs even at energies above 1 GeV. To some extent, discrepancy between the PAMELA and NM spectra may be caused by the flux anisotropy.

The GLE parameters for this event have also been calculated using the NM-BANGLE model (Plainaki et al. 2009a). A direct comparison of the particle fluxes is difficult since these data in Plainaki et al. (2009a) are given only for integral energy spectra (see their Figure 3). An estimation shows that the results of the NM-BANGLE model are very close to the spectra obtained by Vashenyuk et al. (2008a) and therefore differ from the PAMELA results in a similar manner. Figure 4 shows that, during the first polar passage of PAMELA (0318–0329 UT), the Apatity and Barentsburg NMs demonstrated different rate enhancements, i.e., the SEP fluxes were still anisotropic. The NM spectrum refers to the direction of the anisotropy axis where the proton intensity is maximal. The PAMELA viewing directions for the protons below 3 GV (see the lower panel of Figure 8) were not very close to the anisotropy axis, and therefore the PAMELA fluxes may be lower than those derived from NMs. By the next PAMELA polar passage (0406–0420 UT) discrepancy between the PAMELA and NM spectra increased

Table 1
The Best-Fit Parameters of the Solar Proton Spectra in the Energy Interval 80 MeV–4 GeV in the Early Phase of the Event (0318–0349 UT)

Function	A, cm^{-2} sr^{-1} s^{-1} GV^{-1}(GeV^{-1})	Parameters		χ^2/ndf
$A \cdot \exp(-E/E_0)$	(68.2 ± 0.9)	E_0, MeV	(262 ± 2)	3.0
$A \cdot \exp(-R/R_0)$	(179 ± 3)	R_0, MV	(366 ± 2)	7.6
$A \cdot R^{-\gamma-\delta(R-R_0)/R_0}$, $R_0 = 1$ GV	(13.1 ± 0.1)	γ	(2.70 ± 0.02)	4.1
		δ	(1.99 ± 0.06)	
$A \cdot R \cdot (K_2\,(R/c \cdot \alpha \cdot T))^{1/2}$	(106 ± 2)	$\alpha\ T$	(1.71 ± 0.01)	6.4

(Figure 9[b]). Since the flux anisotropy became lower, one should expect better consistency between the PAMELA and NM data. On the contrary, observations show discrepancy that persisted at around 0500 UT (Figure 9[c]). Particle fluxes changed slowly at 0800–1000 UT, so in order to increase statistical significance, the PAMELA results were averaged over 0850–0944 UT (Figure 9[d]). By this time the effect on the NM network was already too small to determine the solar proton spectrum. However, the PAMELA results were confirmed by an independent observation of the Lebedev Physical Institute (LPI) balloon-borne detector (Stozhkov et al. 2007), which measured solar proton energy spectrum in the stratosphere at 0946–1046 UT. Energy of solar protons is determined in the LPI experiment from absorption of protons in the air, so this is also a direct measurement of solar protons, although in a limited energy interval (Bazilevskaya et al. 2010). The good agreement between proton data of the two instruments in the energy range 90 MeV–400 MeV is an additional check that our efficiency and systematics are under control.

5. THE ENERGY SPECTRUM FITTING

The observed spectral shape may give some indications of the acceleration mechanism (Casolino et al. 2008). The proton energy spectrum measured in the early phase of the event, which is closest to the time of primary acceleration (0318–0349 UT), was fitted by the functions representative of various acceleration processes:

$$\Phi_p = A\ e^{-E/E_0} \tag{1}$$

$$\Phi_p = A\ e^{-R/R_0} \tag{2}$$

$$\Phi_p = A\ R^{-\gamma-\delta(R-R_0)/R_0} \tag{3}$$

$$\Phi_p = A\ R\ K_2\ (R/c\,\alpha\,T)^{1/2}, \tag{4}$$

where Φ_p is the proton flux intensity, E is kinetic energy, R is magnetic rigidity, c is particle velocity, and K_2 is a modified Bessel function of the order of 2, with $\alpha\,T$ as free parameter (α representing an acceleration rate and T the escape time from the acceleration region). An exponential in kinetic energy (1) or rigidity (2) function is typical for simple models of DC acceleration (Vashenyuk et al. 2006, 2008a, 2008b), a power law is indicative of shock acceleration (Axford 1981; Krymskii 1977; Ellison & Ramaty 1985), and Bessel function results from stochastic acceleration (McGuire & von Rosenvinge 1984). The best-fit parameters of approximation are presented in Table 1.

It should be mentioned that even if the resulting fits reproduce rather nicely the spectral shape, χ^2 values are high for all of them (see Table 1), showing that these analytical formulas do not correctly describe the spectrum in the whole energy range. The best fit is obtained for the exponential in kinetic energy function (1); however, it fails to describe the highest and lowest energy tails where the observed spectrum is harder (in the $R > 2.5$ GV and $R < 1.7$ GV range). It proves that no single mechanism can describe the SEP energy spectrum in the wide energy interval. The previous successful attempts of the SEP spectra fitting (e.g., Cramp et al. 1997; Vashenyuk et al. 2008a) were possible only for a narrower energy range.

6. DISCUSSION AND CONCLUSION

The PAMELA spectrometer was the first instrument that directly measured the relativistic SEPs in the near-Earth space. It is important since all previous such measurements were fulfilled with a ground-based installation, and the derived SEP fluxes depended on the instrument response functions. The spectra of solar protons in the energy range 80 MeV–3 GeV and helium 75 MeV n^{-1}–1 GeV n^{-1} were measured during the first polar PAMELA passage at 0318–0329 UT. There is a good agreement between the protons fluxes measured by PAMELA and those obtained by the IceTop installation (Abbasi et al. 2008; T. Kuwabara 2009, private communication). Keeping in mind accuracy of the estimation of absolute SEP intensities from the NM data (Vashenyuk et al. 2006; Plainaki et al. 2007, 2009a; Bombardieri et al. 2008), reasonable agreement can be stated between the PAMELA and NM SEP fluxes. However, the PAMELA spectra are always harder in the low-energy interval, probably indicating that NM yield functions are underestimated below ~700 MeV. During the second polar PAMELA passage the difference between the SEP fluxes taken from PAMELA and NMs became larger, while agreement between PAMELA and IceTop remained very good. The correctness of the PAMELA observations was also confirmed by agreement with the direct SEP measurement on a balloon in the atmosphere.

Evolution of the intensity and the spectral shape of relativistic solar protons is often used to derive some information about SEP generation (Bombardieri et al. 2008; Vashenyuk et al. 2006, 2008a, 2008b; McCracken & Moraal 2008; Moraal et al. 2008). Indications were found that the first arriving relativistic particles would be accelerated in the flare region and have an exponential spectrum, whereas the latter particles would be accelerated by a CME-driven shock and have a power-law spectrum. In this case, appropriate dynamics of the energy spectrum could be observed by PAMELA. Being at the low latitudes, PAMELA missed the earliest anisotropic phase of the event of December 13. The results of the first PAMELA observation around 0320 UT on December 13 confirmed the existence of the hard quasi-exponential spectrum expected from the magnetic reconnection in the flare region. However, in spite of changes in the SEP intensity, a quasi-exponential spectrum persisted until the advent

of the newly generated protons of the December 14 event. It should be noted that in the energy interval relevant to the NM observations (> 500 MeV) the spectrum could be fitted by a power-law beginning from ∼1000 UT; however, at lower energies the spectrum was flatter. We did not find any spectral form that would fit the observed spectra satisfactorily in the whole energy range and could prove a certain dominating mechanism of SEP acceleration. A quasi-exponential spectrum and fast temporal evolution of particle fluxes during several hours were present only in the December 13 event when the relativistic protons were generated. In the December 14 event, without relativistic particles, the form of the solar proton energy spectra changed little and was almost a power law throughout the event. In addition, no helium with energy above ∼100 MeV n^{-1} was observed in the December 14 event. This may be indicative of special conditions leading to the acceleration of particles up to relativistic energy.

We acknowledge support from The Italian Space Agency (ASI), Deutsches Zentrum für Luft und Raumfahrt (DLR), The Swedish National Space Board, The Swedish Research Council, the Russian Space Agency (Roscosmos), and the Russian Foundation for Basic Research. We thank the IceTop team and the Polar Geophysical Institute cosmic ray group (Apatity) for providing the IceTop and the NM spectra at the times of PAMELA measurements, the *ACE*/SIS instrument team, and the *ACE* Science Center for providing the *ACE* data. We also thank all people who make their results accessible through the Internet.

REFERENCES

Abbasi, R., Ackermann, M., Adams, J., et al. 2008, ApJ, 689, L65
ACE, C. 2011, ACE Level2 Data, http://www.srl.caltech.edu/ACE/ASC/level2/
Adriani, O., Barbarino, G. C., Bazilevskaya, G. A., et al. 2009a, Nature, 458, 607
Adriani, O., Barbarino, G. C., Bazilevskaya, G. A., et al. 2009b, Phys. Rev. Lett., 102, 051101
Adriani, O., Barbarino, G. C., Bazilevskaya, G. A., et al. 2011, Science, 332, 69
Adriani, O., Bonechi, L., Bongi, M., et al. 2003, Nucl. Phys. B, 125, 308
Agostinelli, S., Allison, J., Amako, K., et al. 2003, Nucl. Instrum. Methods Phys. Res. A, 506, 250
Allison, J., Amako, K., Apostolakis, J., et al. 2006, IEEE Trans. Nucl. Sci., 53, 270
Axford, W. I. 1981, Ann. New York Acad. Sci., 375, 297
Barbarino, G., Boscherini, M., Campana, D., et al. 2003, Nucl. Phys. B, 125, 298
Battistoni, G., Cerutti, F., Fasso, A., et al. 2007, in AIP Conf. Proc. 896, Hadronic Shower Simulation Workshop, ed. M. Albrow & R. Raja (Melville, NY: AIP), 31
Bazilevskaya, G. 2009, Adv. Space Res., 43, 530
Bazilevskaya, G., Makhmutov, V., Stozhkov, Y., Svirzhevskaya, A., & Svirzhevsky, N. 2010, Adv. Space Res., 45, 603
Bieber, J. W., Clem, J., Evenson, P., et al. 2005, Geophys. Res. Lett., 32, L03502
Bieber, J. W., Evenson, P., Drge, W., et al. 2004, ApJ, 601, L103
Boezio, M., Bonvicini, V., Mocchiutti, E., et al. 2002, Nucl. Instrum. Methods Phys. Res. A, 487, 407
Bombardieri, D. J., Duldig, M. L., Humble, J. E., & Michael, K. J. 2008, ApJ, 682, 1315
Casolino, M., Altamura, F., Basili, A., et al. 2006a, Adv. Space Res., 37, 1848
Casolino, M., Altamura, F., Basili, A., et al. 2006b, Adv. Space Res., 37, 1857
Casolino, M., Pascale, M. D., Nagni, M., & Picozza, P. 2006c, Adv. Space Res., 37, 1884
Casolino, M., et al. 2008, Two Years of Flight of the Pamela Experiment: Results and Perspectives, http://adsabs.harvard.edu/abs/2008arXiv0810.4980C
Cramp, J. L., Duldig, M. L., Fluckiger, E. O., et al. 1997, J. Geophys. Res., 102, 24237
De Simone, N., et al. 2009, in Proc. 31th ICRC, Łódź, Poland (http://icrc2009.uni.lodz.pl/proc/pdf/icrc0795.pdf)
Ellison, D. C., & Ramaty, R. 1985, ApJ, 298, 400
Ferrari, A., Sala, P. R., Fassò, A., & Ranft, J. 2005, FLUKA: A Multi-Particle Transport Code, CERN Yellow Report, www.lnf.infn.it/sis/preprint/pdf/getfile.php?filename=INFN-TC-05-11.pdf
Krymskii, G. F. 1977, Akad. Nauk SSSR Dokl., 234, 1306
Laboratory, U. N. R. 2011, Data on Coronal Mass Ejections, http://ares.nrl.navy.mil/cmelist.html
Lee, M. A. 2005, ApJS, 158, 38
McCracken, K. G., & Moraal, H. 2008, in Proc. 30th ICRC, ed. R. Caballero et al. (Vol 1; Mexico City: Universidad Nacional Autonoma de Mexico), 269
McGuire, R. E., & von Rosenvinge, T. T. 1984, Adv. Space Res., 4, 117
Moraal, H., McCracken, K. G., & Stoker, P. H. 2008, in Proc. 30th ICRC, ed. R. Caballero et al. (Vol 1; Mexico City: Universidad Nacional Autonoma de Mexico), 265
NOAA. 2011a, Data of the GOES Satellites, http://spidr.ngdc.noaa.gov/spidr
NOAA. 2011b, International Geomagnetic Reference Field, http://www.ngdc.noaa.gov/IAGA/vmod/igrf.html
NOAA-STP. 2006, X-ray Solar Flare Data, ftp://ftp.ngdc.noaa.gov/STP/.../FLARES_XRAY/2006/xray2006
Papaioannou, A., Mavromichalaki, H., Gerontidou, M., et al. 2011, Astrophys. Space Sci. Trans., 7, 1
Picozza, P., Galper, A. M., Castellini, G., et al. 2007, Astropart. Phys., 27, 296
Plainaki, C., Belov, A., Eroshenko, E., Mavromichalaki, H., & Yanke, V. 2007, J. Geophys. Res., 112, A04102
Plainaki, C., Mavromichalaki, H., Belov, A., Eroshenko, E., & Yanke, V. 2009a, Adv. Space Res., 43, 474
Plainaki, C., Mavromichalaki, H., Belov, A., Eroshenko, E., & Yanke, V. 2009b, Adv. Space Res., 43, 518
Reames, D. V. 1999, Space Sci. Rev., 90, 413
Ricciarini, S. 2007, Nucl. Instrum. Methods Phys. Res. A, 582, 892
Shea, M., & Smart, D. 1982, Space Sci. Rev., 32, 25
Shea, M. A., Smart, D. F., & Gentile, L. C. 1987, Phys. Earth Planet. Inter., 48, 200
Stozhkov, Y., Svirzhevsky, N., Bazilevskaya, G., et al. 2009, Adv. Space Res., 44, 1124
Timashkov, D. A., Balabin, Y. V., Borog, V. V., et al. 2008, in Proc. 30th ICRC, ed. R. Caballero et al. (Vol 1; Mexico City: Universidad Nacional Autonoma de Mexico), 209
Tsyganenko, N. A. 1989, Planet. Space Sci., 37, 5
Tsyganenko, N. A. 2002, J. Geophys. Res., 107, 1176
Tylka, A. J. 2001, J. Geophys. Res., 106, 25333
Vashenyuk, E. V., Balabin, Y. V., Gvozdevskii, B. B., & Karpov, S. N. 2006, Geomagn. Aeron., 46, 424
Vashenyuk, E. V., Balabin, Y. V., Gvozdevsky, B. B., & Shchur, L. I. 2008a, Geomagn. Aeron., 48, 149
Vashenyuk, E. V., Balabin, Y. V., Miroshnichenko, L. I., et al. 2008b, in Proc. 30th ICRC, ed. R. Caballero et al. (Vol 1; Mexico City: Universidad Nacional Autonoma de Mexico), 253